Interaction between Longitudinal Acoustic Waves and Sidewall Injection in a Cavity (Slender Chamber)

A. M., Hegab[#1]

Mechanical Engineering Department, Faculty of Engineering at Rabigh,King Abdulaziz University, Saudi Arabia

Abstract *In this paper, analytical and computational studies are employed to examine the interaction between the generated longitudinal acoustic waves and the injected fluid from the sidewall in slender chamber. This wave pattern mechanism may lead to an intense unsteady vorticity with associated shear stresses in real rocket chamber. The mass injection and the generated end-wall disturbance may mimic the unsteady burning processes at resonance and non-resonance frequencies. The analytical approach is formulated using asymptotic technique to reduce the full governing equations. The results show that unexpectedly large amplitude of unsteady vorticity are generated at the injection sidewall of the chamber and penetrated downstream by the bulk motion of the internal flow. These stresses may cause scouring effect and large transient heat transfer on the combustion surface. A comparison between the three adapted approaches is presented*.

Keywords *Acoustic Waves, Solid Rocket Motor Chamber, Sidewall Injection, and Perturbation Analysis.*

Nomenclature

x	Dimensionless chamber length
y	x'/L'
	Dimensionless chamber heigh
	y'/H'
T	Dimensionless Temperature
u	T'/T'$_o$
v	Dimensionless velocity in x-Dir. u'/U'$_{zo}$
p	
t	Dimensionless velocity in y-Dir. v'/(U'$_{zo}$/δ□
E_t	Dimensionless pressure p'/p_o
	Dimensionless time t'/t'$_a$,
	t'$_a$=L'/C'$_o$
	Total Energy
	$\rho[T+\gamma(\gamma-1)M^2(u^2+(v/\delta)^2]$

Greek Symbols

Ω	Dimensionless vorticity
ε	Amplitude of endwall
λ	disturbances
δ	Chamber natural frequency
	Aspect ratio L/H
Ω	Dimensionless forcing frequency

Subscripts

os	Steady State
w	Wall conditions
n	Eigenvalues
0	First fundamentals
O	Reference values
A	acoustic

Exponents

*	Resonance conditions
~	Perturbed values
,	Dimensional values

Non-dimensional Numbers

Reynolds number,

Re $R_e = \frac{\rho_o' U_{z_o}' L'}{\mu_o'}$, and $R_{ea} = \frac{R_e}{M}$

R_e=O(10^5-10^6)

Characterstics Mach

M number $M = \frac{U_{z_o}'}{C_o'}$

M≤ O(10^{-1})

P_r Prandtl number $\frac{\mu_o' C_{P_o}'}{k_o'}$,

.

I. INTRODUCTION

The propagation of acoustic waves (irrotational field only) in closed or open end tubes without any consideration for the mass injection from the sidewall have been studied intensively by the experimental and theoretical approaches, [1-10]. These studies described the behaviour of finite amplitude waves at or near resonance frequencies and the effect of nonlinearity on the waveform. Erickson et al. [1] studied theoretically the behaviour of forced finite amplitude oscillations in cylindrical constant and variable area ducts whose ends are closed. Shock waves are observed in the form of saw-tooth like waveforms in the case of constant area duct when the duct oscillate at resonance frequency. Similar theoretical and experimental works are carried out by Zapirov and Ilhamov [2]. Merkli and Thomann [3] studied experimentally the thermo-acoustic effects in resonant closed tube. Their results showed the steepness of the wave and the shock wave formation near or at the resonance frequencies.

In the present paper analytical, computational, and experimental studies are performed to describe the nature of a low Mach number and weakly viscous flow field generated in a long, narrow chamber with steady sidewall mass injection and endwall disturbances. The inviscid rotational steady injected flow interacts with the irrotational acoustic field to generate unsteady vorticity at the sidewall and is penetrated toward the centerline by the steady transverse velocity component. The axially distributed transverse velocity on the sidewall is a prescribed and the temperature of the injected gas is specified.Studies of time-dependent, compressible internal fluid dynamics in semi confined geometries as a cold flow models are often motivated by the need to explain flow processes in real solid rocket motor chambers. In particular, the models incorporating explicit axial distributions of transient mass addition on the sidewalls are used to mimic the impact of unsteady propellant burning on the acoustic and flow dynamics in the motor chamber. Our recent studies that incorporate a combustion process of microscale solid rocket motor propellant for the sandwich models by Hegab et.al.[1,2], and for the composite propellant by Buckmaster et.al. [3], Kochevets et.al.[4] revealed that the boundary conditions, in particular at the injection surface of the cold model simulations differ from those found with the combustion models. As a results, we try in this study to specify axial distributions of the transient velocity injection on the sidewall with different wave numbers to simulate the corregation that arises from the burning of composite propellants.

1) 2. The Mathematical Formulation

2.1. Governing Equations

The mathematical model is based on the following;

$$\frac{\partial Q}{\partial t}+\frac{\partial E}{\partial x}+\frac{\partial F}{\partial y}=0 \quad , \qquad \textbf{(1)}$$

$$Q=\begin{bmatrix}\rho\\ \rho u-\\ \rho v-\\ E_T-\end{bmatrix}, \quad E=\begin{bmatrix}M\rho u\\ M\rho u^2+\frac{1}{\gamma M^2}p\\ M\rho uv-\\ M\{E_T+(\gamma- \quad 1)p\}u-\end{bmatrix},$$

$$F=\begin{bmatrix}M\rho v\\ M\rho uv-\frac{\delta^2 M}{R_e}u_y\\ M\rho v^2+\frac{\delta^2}{\gamma M}p\\ M\{E_T+(\gamma-1)p\}v-\frac{\gamma\delta^2 M}{R_e P_r}T_y\end{bmatrix}$$

2.1.1. The Analytical Approach

The steady state variables for the incompressible, inviscid, rotational flow can be described using the asymptotic expansions as

$$(u,v)\approx\sum_{i=0}M^i(v_{is},\ u_{is}) \qquad \textbf{(2)}$$

$$(p,\ \rho\ ,T)\approx 1+\sum_{i=0}M^{i+2}(p_{is},\ \rho_{is},\ T_{is}) \qquad \textbf{(3)}$$

The solution to the first order calculations that satisfies the boundary conditions of the assigned rocket chamber can be written as:

$$v_{os}=-V_w(x)\sin(\pi/2y) \qquad \textbf{(4)}$$

$$u_{os}=\left(\frac{\pi}{2}\int_0^x V_w(\tau)d\tau\right)\cos(\pi/2y) \qquad \textbf{(5)}$$

$$p_{os}=\frac{\gamma\pi^2}{4}\int_x^1\left[V_w(x)\int_0^x V_w(\tau)d\tau\right]dx \qquad \textbf{(6)}$$

While the perturbation values is derived as follow;

$$\tilde{u_0}(x,t)\Big|_{n\neq n^*}=\varepsilon\sin\omega t+\sum_{n=0,n\neq n^*}^{\infty}-2\frac{\varepsilon\omega}{\lambda_n^2}\sin\lambda_n t\sin\lambda_n x$$
$$+\sum_{n=0,n\neq n^*}^{\infty}\left\{-2\frac{\varepsilon\omega^3}{\lambda_n^2(\lambda_n^2-\omega^2)}\sin\lambda_n t+2\frac{\varepsilon\omega^2}{\lambda_n(\lambda_n^2-\omega^2)}\sin\omega t\right\}\sin\lambda_n x \qquad \textbf{(7)}$$

The resonance solution when

$$\omega=\lambda_n^*$$

is derived and written as;

$$\tilde{u_0}(x,t)\Big|_{n=n^*}=\varepsilon\sin\omega t-\left(\left\{\frac{1}{\lambda_n^*}\right\}\sin\lambda_n^* t+t\cos\lambda_n^* t\right)\sin\lambda_n^* x \qquad \textbf{(8)}$$

2.2 The Computational Approach

A finite difference techniques are used to solve the full Navier-Stokes equation in a cavity open from one side and closed from the other side. This scheme shows the evolution of flow variables across the whole chamber after many acoustic wave cycles. The present finite difference approach is employed to reduce the impact of numerical instabilities found to affect results obtained from a second order explicit MacCormack code, Kirkkopru, et al. [15]. Near the boundaries, the second order explicit predictor-corrector scheme, developed by MacCormack[16] is used to solve the 2-D, unsteady, compressible Navier-Stokes equations. At the interior points, the Navier-Stokes equations are solved numerically using the Two-Four explicit, predictor-corrector scheme, developed by Gottlieb et al.[17] which is a fourth-order variant of the fully explicit MacCormack scheme. This method, applied by Hegab, [13], Hegab, et.al. [14], and Kirkkopru et al.[15], is phase accurate and therefore suitable for describing many wave cycles and wave interaction problems. The grid points are equally spaced in each direction within the chamber. The number and spacing of the grid

points used defines the accuracy and resolution of the local variations of flow variables in the axial and transverse directions

3. Code Validation

Our results have been classified into three categories. "The first category of the computational and analytical results deals with the steady state flow solutions that is generated by a constant side wall mass injection (Vrw=-1) from the upper side of the chamber. The experimental results for the steady state flow by Deng, et.al. [19,20] are compared with the current mathematical models in order to validate the computational approach for the steady state solution. The second set of the results show the solution for the unsteady flow computations. A comparison between the asymptotic analysis and the computational solution for the weakly rotational equations is presentedin figure (1). The last set of the results are from the computational approaches to study the generation and convection of vorticity and temperature flow dynamics due to the interaction between the acoustic disturbances that arises from the unsteady mass injection and the injected fluid.

The first set of the results show the converged steady state solutions with constant sidewall injection at a given values of M, Re, and δ. The normalized axial velocity profiles across the mid-length of the chamber are presented in figure (1). The solid line represents the asymptotic analysis solution, for the steady, incompressible, inviscid flow. The dotted line refers to the computational solution for converged steady, compressible, viscous flow with Re=105 (Rew=5*10^3). The unfilled points with no-lines represent some of the experimental results carried out by Deng, et.al. [21,22] for the flow in a channel with fully transpired wall of three different porous surface using three different sizes of honeycomb cells. The geometry of Deng and coworkers channel is rectangular with dimension of total length L' ~1600 mm, and channel height ~ 77 mm. Therefore the aspect ratio L'/H' is about twenty, which is similar to the aspect ratio in the current physical model. In addition, the dimensional flow characteristics in the current model are nearly fit the dimensional flow characteristics of the experimental work. For example, in the computational model the characteristics Mach and injection Reynolds numbers are chosen to be M~ O(10^{-2}), and Re|injection=Rew=Re/δ~O(10^3) respectively. Since, M=U'zo/C'o, then the characteristics mean axial flow velocity exit from the chamber U'zo varies from 3.5-7.5 m/s and, in turn, by equating the total mass injected from the side wall with the total mass exit from the chamber, the injection characteristics velocity V'yo ~ U'zo/(L'/H') ~ 0.175 – 0.35 m/s. These ranges of the injection and exit dimensional velocities meet the experimental measurements when they used the smallest pore size of the honeycomb 1/8" surface. The experimental approach by Deng, et.al. is used 2D Laser Particle Image Velocimetry (PIV) to measure the instantaneous flow fields across the channel. The mean flow properties and statistics are obtained by analyzing the instantaneous measurements. At the midlength of the chamber, a comparison between the asymptotic analysis velocity profile and the computational converged steady state velocity profile with the experimental results shows a reasonable agreement with a certain deviation between the experimental and the theoretical approach. This deviation goes smaller and smaller as the injection Reynolds number becomes closer to the theoretical one".

Figure (1) : Normalized axial velocity profiles at the midlength of the chamber for the steady state flow, [22].

The steady state velocity vector map at t=0 is presented in Fig. (3). The upper side of the map is located very close to the injection surface, where the flow is completely vertical with a constant injection velocity V_{rw}=-1. The left hand side of the map represents the

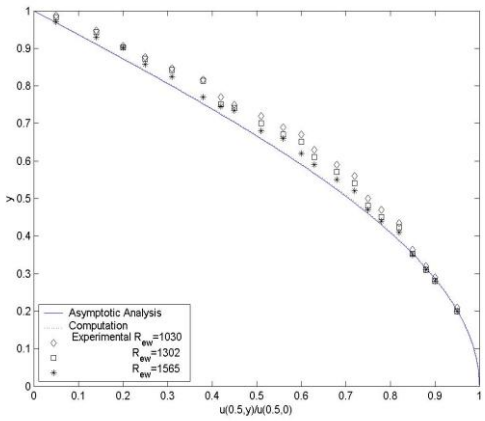

closed end of the channel, where u=0.0 and the total velocity (VT =v(0,y)) varies in a vertical direction ($\theta=90^o$) from Vrw at the wall to zero at the centerline. The bottom side of the map draws the flow field along the centerline, where the flow is completely axial, $\theta=0.0^o$ and $V_T=u(x,0)$ which varies from zero at the head end to the maximum limit at the open end. The right hand side of the map represents the open end of the channel, where the flow is completely axial. At any points elsewhere in the domain the length and the angle of the vector map lines scales the magnitude and the direction of the total velocity at that point. It is noted that these vectors is qualitatively closer to the experimental flow pattern by Deng, and the coworker in particular in case of less turbulence with the pore size 1/8" honeycomb. These figures don't appear any acoustics disturbances, since the source of the unsteady injection is still steady.

4. Results and discussions

In this study the asymptotic methodologies is combined with the numerical approaches to give precise fundamental insights for the unsteady flow dynamics in a chamber with endwall disturbances and steady sidewall injection. The current results have been classified into two categories. The first category of the results deals with the acoustic fields in the chamber without injection from the sidewall using the computational and analytical approaches. The second set of the results show the solution for the unsteady flow computations. A comparison between the asymptotic analysis and the computational solution for the weakly rotational equations is presented.

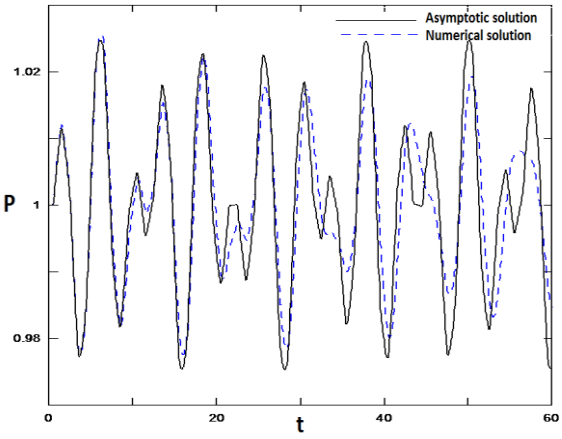

Figure(2): Comparison between the computational and analytical results for the pressure time history at the medlength of the chamber, ε= 0.1 , ω = 1.0 (f`=159 Hz).

Figure 1 illustrates a comparison between the computational and analytical results for the pressure time history at the medlength of the chamber, ε= 0.1 , ω = 1.0 (f`=159 Hz). A good agreement is found for the t<20, while the deviation found to be significant as time increases. Figure (3): The vorticity topography for $Re=3*10^5$, M=0.01, δ=20, and ε=0.4 at t= 8, 16, 32 and 40. It is clearly seen from this figure that the unsteady vorticity and the associated shear stresses is generated at the combustion surface in real rocket chamber and is the spreading to fill the entire chamber as time increases. The locations of the vorticity fronts is very close to the analytical solution in [11], and applied by [12-14], equation (9);

$$\Omega_e(t)=\frac{2}{\sqrt{\pi}}\left(\tan^{-1}\left(e^{-M\pi t}\right)\right)^{1/2} \quad (9)$$

Comparison between the analytical solution and the computational solution for the vorticity edge at M=0.01, Re = 3*105, ε=0.4, and ω=1 is presented in figure (2)

.

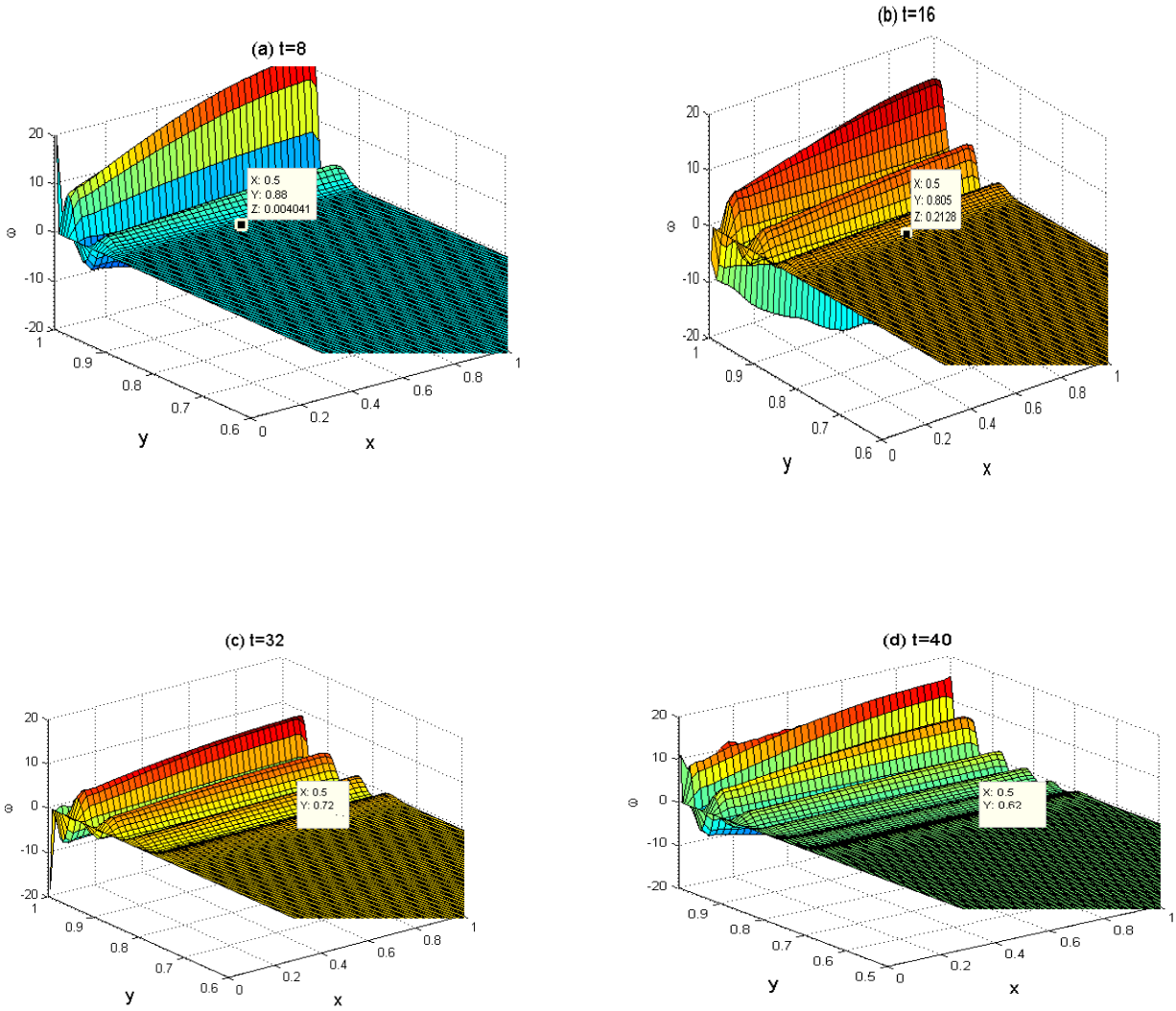

Figure (3): The vorticity topography for Re=3*105, M=0.01, δ=20, and ε=0.4 at t= 8, 16, 32 and 40.

In the context of propellant combustion, one may anticipate that the intensive unsteady vorticity generation and the associated shear stresses will persist to the surface of a burning solid propellant in a real rocket chamber and are likely to impact the characteristics of the combustion process

Table (1) : Comparison between the analytical solution and the computational solution for the vorticity edge at M=0.01, Re = 3*105, ε=0.4, and ω=1

Time	Analytical Unsteady vorticity front $\Omega_e(t) = \frac{2}{\sqrt{\pi}}\left(\tan^{-1}\left(e^{-M}\right.\right.$	Computational vorticity front	Deviation	Percentage (%)
t=0	1.0	1.0	0	0 %
t=8	0.902	0.880	0.02	2.21 %
t=16	0.835	0.805	0.03	3.59 %
t=32	0.679	0.720	-0.041	- 5.2 %
T=40	0.60	0.621	-0,021	- 3.33 %

5. Conclusion

The current paper is designed to examine the complex wave pattern and its interaction with the mass injection from the sidewall. The latter represents or mimics the real burning of solid rocket propellant. In the context of propellant combustion, one may anticipate that the intensive unsteady vorticity generation and the associated shear stresses will persist to the surface of a burning solid propellant in a real rocket chamber and are likely to impact the characteristics of the combustion process

References

[1] Erickson R., Markopoulos N., and Zinn, B. "Finite Amplitude Acoustic Waves in Variable Area Ducts" AIAA-01-1099, 39th AIAA Aerospace Sciences Meeting and Exhibit, , 8-11 January 2001, Reno, NV, USA.

[2] R.G. Zaripov and M. A. Ilhamov 'Nonlinear Gas Oscillations in a Pipe' J. Sound vol.., 46, pp 245-257, (1976)

[3] P. Merkli and H. Thomann " Thermoacoustic Effects in a Resonance Tube" J. Fluid Mech., V.70, pp.161-177, July 1975

[4] Meng Wang and D.R. Kassoy " Nonlinear Oscillation in a Resonant Gas Column: An Initial-Boundary Value Study" SIAM J. Appl. Math., V.55, No. 4, pp. 923-951, August 1995

[5] J. Jimenez ' Nonlinear Gas Oscillation in Pipes. Part1. Theory' J. Fluid Mech.(1973), Vol. 59, part 1, pp.23-46

[6] Ahmed A. Sileem" Nonlinear Evolution of Resonant Acoustic Oscillations in a Tube Ended With Variable Area Portion" International Conference on Energy Research & Development (ICERD, Nov., 9-11-1998), Kuwait, pp

[7] Ahmed A. Sileem and M. Nasr, "An Experimental Study on Finite Amplitude Oscillations in Ducts: The Effect of Adding Variable Area Part to The Open End of Constant-Area Resonant Tube", Alexandria Engineering Journal, Faculty of Engineering Alexandria University, EGYPT, pp 397- 409, Vol 42, No. 4, January 2003.

[8] Brian R. Seymour and Michael P. Mortell ' Resonant Acoustic Oscillation with Damping: Small Rate Theory' J. Fluid Mech.(1973), Vol. 58, part 2, pp.353-373

[9] J.H.M. Disselhorst and L. Van Wijngaarden 'Flow in the Exit of Open Pipes during Acoustic Resonance' J. Fluid Mech. (1980), vol. 99, part 2, pp. 293-319.

[10] J. E. Garcia-schafer and A. Linan. "Longitudinal acoustic instabilities in slender solid propellant rockets: Linear analysis" J. Fluid Mech. (2001), vol. 437, pp.229-254

[11] Zhao, Q., Staab, P.L., Kassoy, D.R., and Kirkkopru, K. (2000), "Acoustically Generated Vorticity in an Internal Flow," J. Fluid Mech., #13, 247-285

[12] Hegab, A.M., Kassoy, D.R. (2006) "Internal flow temperature and vorticity dynamics due to transient mass addition AIAA Journal, 44 (4), pp. 812-826

[13] A. M. Hegab, H. H. Sait, A. Hussain, 2014 "IMPACT OF THE SURFACE MORPHOLOGY ON THE COMBUSTION OF SIMULATED SOLID ROCKET MOTOR", Mathematical Problems in Engineering Volume 2015, Article ID 485302, 11 pages, http://dx.doi.org/10.1155/2015/485302

[14] Hegab, A.M. Vorticity generation and acoustic resonance of simulated solid rocket motor chamber with high wave number wall injection (2009) Computers and Fluids, 38 (6), pp. 1258-1269.

[15] Kirkkopru, K., Kassoy, D.R., and Zhao, Q. (1996), " Unsteady Vorticity Generation and Evaluation in a Model of Solid Rocket Motor," J. of Propulsion and Power, **12**, No. 4, 646-654.

[16] MacCormack, R.W. (1982), " A Numerical Method for Solving the Equations of Compressible Viscous Flow," AIAA J., **20**, No. 9, 1275-1281.

[17] Gottlieb, D., and Turkel, E. (1976) "Dissipative Two-Four Methods for Time-Dependent problems," Mathematics of Computation, **30**, No. 136, 703-723.

[18] Deng, Z., Adrian, R.J., Tomkinsm C.D. (2001), "Structure of Turbulence in Channel Flow with a Fully Transpired Wall", AIAA Paper 2001-1019, 39th Aerospace Science Meeting ,Reno, NV.

[19] Deng, Z., Adrian, R.J., Tomkinsm C.D. (2002) "Sensitivity of Turbulence in Transpired Channel to Injection Velocity Small-Scale Nonuniformity", Journal of AIAA, Vol. 40, No. 11, November, 2002.

[20] Culick, F.E.C. (1966), "Rotational Axisymmetric Mean Flow and Damping of Acoustic Waves in a Solid Propellant Rocket," AIAA J. 4, No. 8, 1462-1464.

[21] A.M. Hegab, Vorticity Generation and Acoustic Resonance of Simulated Solid Rocket Motor Chamber with High Wave Number Wall Injection, J. of Computers & Fluids, Vol. 38(2009) 1258-1269.

[22] Anoop Thankachen, Santosh kumar, (2015), "Design Optimization and Analysis of Rocket Structure for Aerospace Applications", Volume-24 Number-6, International Journal of Engineering Trends and Technology (IJETT)